Novel Synchronous Reluctance Motor with Sinusoidal Rotor Lamination Shape for Less Torque Ripple Contents

Journal:	*IEEE Transactions on Energy Conversion*
Manuscript ID	TEC-00778-2017
Manuscript Type:	Transactions
Date Submitted by the Author:	07-Oct-2017
Complete List of Authors:	MUTEBA, MBIKA ; University of Johannesburg - Doornfontein Campus, Electrical and Electronic Engineering Technology TWALA, BHEKISIPHO; University of Johannesburg - Doornfontein Campus NICOLAE, DAN ; University of Johannesburg - Doornfontein Campus, Electrical and Electronic Engineering Technology
Technical Topic Area:	Switched and variable reluctance machines < Electric Machinery
Key Words:	AC motors, Reluctance motors, Torque, Finite element methods

Novel Synchronous Reluctance Motor with Sinusoidal Rotor Lamination Shape for Less Torque Ripple Contents

M. Muteba, *Member, IEEE*, B. Twala, *Member, IEEE*, and D. V. Nicolae, *Member, IEEE*

Abstract— **This paper presents the analysis of a novel Synchronous Reluctance Motor (SynRM), which has an axially sinusoidal rotor lamination shape. The sinusoidal lamination shape is used to vary magnetic flux in the *q*-axis direction. Therefore, cancelling some torque harmonics produced by stator slotting effects and rotor anisotropy, while maintaining the average torque. The stator of a 5.5 kW, 4-pole, 50 Hz conventional three-phase squirrel cage induction motor, with distributed and chorded by one slot, double layer winding, is used for both standard and novel motors. The Finite Element Analysis (FEM) is used to study the electromagnetic parameters of interests. The FEA results are validated by means of practical measurements. The results obtained from both FEA and practical measurements evidenced that the novel SynRM dropped tremendously the torque ripple contents while still maintained the average torque. The drop in torque ripple contents is mainly due to mitigation of the most dominant torque harmonics caused by stator slotting and rotor anisotropy.**

Index Terms— **High average torque, low torque ripple, novel rotor with sinusoidal shape, synchronous reluctance motor.**

I. Introduction

THE major behavior and characteristics of an anisotropic structure suitable for high performance SynRM rotor geometry design is discussed in [1] and [2]. The design concept that enhances the rotor anisotropy for high performance is based on the combination of different work in [3], [4], [5], [6], [7], [8], [9] and [10]. The complexity of the SynRM rotor structure and the presence of microscopic geometrical parameters make the design and its optimization difficult [1].

Previous work that attempted to address the complex nature of the problem can be found in the works of Vagati, Lipo, Boldea, Kamper, Fratta, Lovelace, Talebi, Bianchi and Toliyat [6], [7], [11], [12], [13], [14], [15], [16]. Despite the complex nature of rotor geometric parameters, the SynRM is a good competitor in applications that require high torque density, fault-tolerant capability and low rotor inertia [17]. Despite several advantages, one of common problems of SynRMs is the high content of torque ripples [2]. This is due to the interaction between spatial harmonics of the electrical loading and the rotor anisotropy which causes a high torque ripple that is intolerable in most applications [2].

Several efforts have been made to mitigate torque ripples in SynRMs. In 2002, Bomela reported that the skewing of the rotor by a stator slot pitch reduces the slot torque harmonic, but it also drops the average torque [18]. A few years earlier (1997), Vagati indicated that a reduction of torque ripple can be achieved by means of a suitable choice of number of flux-barriers with respect to the number of stator slots per pole pair. The flux-barrier ends are uniformly distributed along the airgap, similarly to the stator slot distribution [19]. Before that (1993), Fratta devided the the SynRM rotor into two sections that are shifted with respect to each other by a proper angle. This has assisted the compensation of one harmonic component [9]. Three years later (1996), through a multi cross-sectional 2D Finite Element Analysis (FEA), Chiricozzi skewed the rotor by means of stacking it in four parts with no parallel flux barrier. This was meant to minimize the inductances as they significantly affect the static torque [20].

The use of asymmetric flux barrier arrangement as a meams of improving torque ripple of the SynRM was first reported in 2003 by Sanada [21]. The method consists of shifting the relative position between the edge of each flux barrier and stator teeth by a certain angle. Most recently (2014), asymmetric flux barrier angles and a flipped rotor structure have been presented by Lange as an approach to reduce torque ripple in SynRMs without losing the average torque [22].

Elsewhere a novelty strategy to compensate the torque harmonics of the SynRMs has been presented by Bianchi and peers. The method is achieved by forming a rotor with two different types of laminations called “Romeo (R-type) and Juliet (J-type)” [14], [17].

The focus of previous work intended to reduce the torque ripple contents of synchronous reluctance motors was focused mostly on a suitable choice of number of flux-barriers with respect to the number of stator slots per pole per phase; the optimization of the flux-barriers geometry; the use of asymmetric flux barrier angles and different asymmetric rotor structures. While some methods are found to have reduced the torque ripple, they also dropped the overall average torque. Other methods that reduced the torque ripple and maintained the average torque at the same time were found to have been assisted by a permanent magnet.

II. Design of the Novel SynRM

A. Background

In 2014, Zhao proposed and analyzed the material-efficient Permanent Magnet Synchronous motor with a sinusoidal magnet shape. The magnet shape provides a sinusoidal magnetic flux in order to obtain better sinusoidal

electromotive force, less cogging torque and smoother electromagnetic torque [23]. The analysis was performed on fraction of Horse power (Hp) permanent magnet surface-mounted motors used in automotive actuators. For a total rotor volume of 86.6 cm^3, the magnet volume of 18.2 cm^3 for the proposed Permanent Magnet Synchronous motor with sinusoidal magnet shape was obtained.

Although, both Finite Element Analysis (FEA) and practical results presented by Zhao are satisfactory, the use of the proposed motor is limited to a fraction of Hp application. For medium and high power motors to be used in traction, electric vehicles and hybrid electric vehicles, where less torque ripple and high torque density are required, the magnet volume will be intolerably high.

In this paper, the design and analysis of the novel SynRM with the sinusoidal lamination rotor shape in the axial direction, without changing the flux barrier geometry, are presented. The idea is inspired from the work done by Zhao and peers regarding the material-efficient Permanent Magnet Synchronous motor with sinusoidal magnet shape [23]. The SynRM with sinusoidal rotor shape was first reported in 2016, and the study was done on a 1.5 kW, six-pole machine and it was only limited to only FEA [24].

B. Design of basic variables

Fig.1 (b) illustrates the cross-section of basic SynRM with cut-off on q-axis, while Fig 1 (a) shows the photograph of the prototype for the standard rotor without cut-off oh the q-axis. Table 1 depicts the general design specifications for a 4-pole, 5.5 kW SynRM with 36 stator slots.

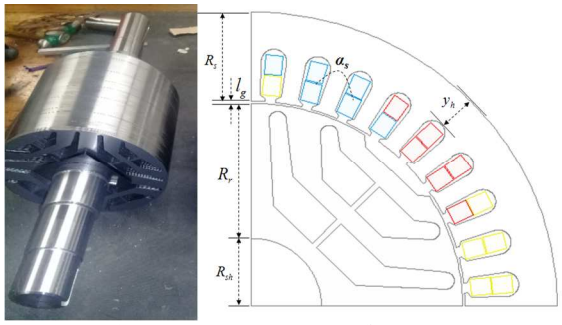

(a) (b)

Fig.1: Standard SynRM, (a) Photograph of the prototype rotor without cut-off, (b) cross section of the standard SynRM with cut-off on the q-axis

TABLE I
GENERAL DESIGN SPECIFICATIONS

Description	Values
Stator slot α_s	10^o *mech*
Airgap length l_g	0.88 mm
Stack length Z	160 mm
Number of barriers per pole	2
Number of pole pairs p	2
Number of stator slots Q_s	36
Rotor radius R_r	48.80 mm
Stator radius R_s	31.62 mm
Shaft radius R_{sh}	24.00 mm
Yoke height y_c	12.87 mm

B. Design concept of the novel SynRM

The general design specifications and the rotor design main variables for the novel SynRM are given in Table 1. The cross-section, the 3D view and the photographs of the prototype novel rotor with sinusoidal rotor shape are shown in Fig.2. The proposed novel rotor consists of stack laminations with identical flux barriers and different cut-off specifications on the q-axis. While the cut-off height (h_c) is kept constant, the cut-off angle (α_c) and cut-off pitch angle (τ_p) near the airgap, along the q-axis direction, are varied. The cut-off pitch is varied by a fifth of the stator slot pitch and the cut-off angle is varied by a relatively small value as given by (1) and (2). The variation of cut-off pitch and cut-off angle for one half period of the sinusoidal structure are expressed as

$$\tau_{pk} \in \left[\frac{5\alpha_s}{2}, \frac{\alpha_s}{4}\right] \quad (1)$$

$$\alpha_{ck} \in \left[\frac{\alpha_s}{5}, \frac{\alpha_s}{10}\right] \quad (2)$$

where k represents the stack lamination number, α_s is the stator slot pitch, τ_{pk} is the cut-off pitch in mechanical degree for lamination "k" and α_{pk} is the cut-off pitch angle in mechanical degree for lamination "k". For k_1, the cut-off pitch τ_{p1} is 25^0 *mech*.

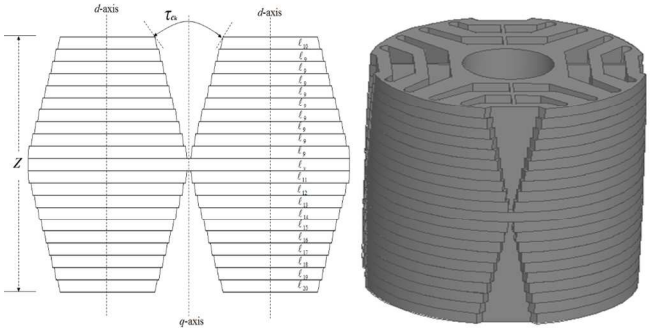

(a) (b)

(c)

Fig. 2: Rotor of the Novel SynRM, (a) cross-section, (b) 3D view, (c) photographs of the prototype novel SynRM rotor

From Fig.2, it is noted that the variation of the cut-off pitch angle results in step-changing of the cut-off base lengths, thus forming a sinusoidal shape along the axial length of the rotor. The total axial length of the rotor lamination is equal to

$$Z = 2(g_1 + g_2 + g_3 ... + g_k) + g_\upsilon + w_i \quad (3)$$

Here w_i is the total thickness of steel lamination insulation coating, g_υ is the axial length of the middle lamination shape and g_k is the axial length of each k individual lamination shape in one half period of the sinusoidal structure. It should be noted that the middle stack lamination shape has no cut-off angle at all and isolates the two adjacent periodical structures.

III. Torque Ripple Harmonic Cancelation

The torque equation of a SynRM that accounts the dependency of inductances as function of rotor position is given by [10]

$$T(\theta) = \frac{3}{2}\frac{p}{2}[(L_{do} - L_{qo})i_d i_q + (\Delta L_d + \Delta L_q)i_d i_q \cos(3pq\vartheta_r) - \Delta L_{dq}(i_d^2 - i_q^2)\sin(3pq\vartheta_r)] \quad (4)$$

where q is the number of slots per pole per phase, ΔL_d and ΔL_q are the variation of the d- and q-axis synchronous inductances respectively, and ΔL_{dq} is the variation of d-q inductances.

In (4), the main torque and the ripple components are shown. The torque ripple has two components; the first one has the coefficient cos ($3pq\vartheta_r$) that gives a ripple proportional to the average torque, while the second one has the coefficient sin ($3pq\vartheta_r$) which is responsible for no-load condition ripple [2]. In the first component of the torque ripple, ΔL_d is caused by the oscillation of the Carter's factor, while ΔL_q is mainly related to oscillation of the circulating flux component along the q-axis [10].

The torque harmonic produced by the variation of d-axis inductance (ΔL_d) and q-axis inductance (ΔL_q) along the positive half period of the sinusoidal structure is the same in magnitude with the harmonic torque produced in the negative half period [24]. The middle stack lamination has no-cut-off, the effect of ΔL_d and ΔL_q can be negligible; the effect on other rotor stack laminations that form the sinusoidal shape will be cancelled due to the opposite periodicity of the rotor structure [24]. Neglecting the first component of torque ripple in (4), the torque equation for Novel SynRM with sinusoidal shape is then expressed by

$$T(\theta) = \frac{3}{2}\frac{p}{2}[(L_{do} - L_{qo})i_d i_q - \Delta L_{dq}(i_d^2 - i_q^2)\sin(3pq\vartheta_r] \quad (5)$$

The only term that will be highly responsible for torque ripple production is ΔL_{dq}. For the proposed Novel SynRM the cut-off pitch is varied, thus reducing the insulation on the q-axis and increasing the iron on the d-axis in the first half period as noticed in Fig.4. The action is reversed in the second half period, where the iron on the d-axis is reduced and insulation increased on the q-axis. The ΔL_{dq} is therefore varied, and this variation contributes to the cancellation of some torque harmonics when the rotor sweeps through certain angular positions.

A. Effect of stator slot opening and rotor cut-off opening

It was noted in the previous section that the variation of ΔL_{dq} contributes to the cancellation of some torque harmonics when the rotor sweeps through certain angular positions. In order to clearly elaborate the effect of ΔL_{dq}, the airgap flux density distribution should be analyzed with the Carter's coefficients in mind due to stator slot opening and rotor cut-off opening. Under no-load condition, the airgap flux density can be computed as the product of the MMF and the inverse airgap length l_g at a rotor position ϑ according to [25]

$$B(\vartheta, t) = \mu_o F(\vartheta, t)\frac{1}{l_g(\vartheta)} \quad (6)$$

The rotor of the Novel SynRM has a variation of cut-offs on the q-axis. The mid-point stack lamination does not have any cut-off; it is equivalent to a round rotor. The Carter's factor should be unity for the mid-stack lamination according to the expression of the Carter's coefficients based on conformal transformation, traditionally used in the absence of saturation [26], [27] and given from (7) to (9). But the Carter's factor cannot be unity due to high flux density saturation in the thin tangential bridges that causes the flux density not to be uniformed.

$$\kappa_{cs} = \frac{\tau_s}{\tau_s - \gamma_s l_g} \quad (7)$$

$$\kappa_{cr} = \frac{\tau_r}{\tau_r - \gamma_r l_g} \quad (8)$$

$$\kappa_c = \kappa_s \kappa_r \quad (9)$$

Where K_{cs} and K_{cr} are the Carter's coefficients due to stator slot opening and rotor cut-off opening respectively, and K_c is the Carter's factor. The factor γ was given by Carter in 1926 and it is obtained by using [28]

$$\gamma_{s,r} = \frac{4}{\pi}\left[\frac{b_{o(s,r)}}{l_g}\arctan\left(\frac{b_{o(s,r)}}{l_g}\right) - \ln\sqrt{1 + \left(\frac{b_{o(s,r)}}{l_g}\right)^2}\right] \quad (10)$$

Here $b_{o\,(s,r)}$ is the stator slot opening "s" or rotor cut-off opening "r". Disregarding the stator slotting, the product $\mu_o F(\vartheta, t)$ in (6) is also unity and the airgap flux density at a point of the rotor position ϑ of the middle lamination is expressed as

$$B_{g\upsilon}(\vartheta) = \frac{1}{l_g(\vartheta)} = f_s(\vartheta) \quad (11)$$

The airgap conductance of the mid-stack lamination at rotor position ϑ is given by

$$\sigma_{\upsilon}(\vartheta)=\frac{1}{l_g(\vartheta)}=\mathrm{f}_s(\vartheta) \tag{12}$$

The stator slotting is not disregarded in FEA. The physical airgap length l_g cannot be used since the stator is slotted. Let $\Delta l_{g_s}(\vartheta)$ be the increase in airgap length due to stator slot opening. At any given point, the fictitious (effective) airgap length $l_{g\upsilon_{eff}}(\vartheta)$ with mid-point rotor stack lamination can be expressed as

$$l_{g\upsilon_{eff}}(\vartheta)=\Delta l_{g_s}(\vartheta)+l_g \tag{13}$$

$$\Delta l_{g_s}(\vartheta)=l_{g\upsilon_{eff}}-l_g=\frac{1}{\mathrm{f}_s(\vartheta)}-l_g \tag{14}$$

Taking into account the stator slotting effect by the use of the Carter's coefficient, the effective airgap length with the mid-point rotor stack lamination is given in (15) and the increase in airgap due to stator slot opening, with the mid-point rotor lamination stack can also be expressed as in (16).

$$l_{g\upsilon_{eff}}(\vartheta)=l_g\,\kappa_{cs} \tag{15}$$

$$\Delta l_{g_s}(\vartheta)=l_g(\kappa_{cs}-1) \tag{16}$$

The rotor is not round for the rest of the rotor stack laminations, which have different cut-offs on the *q*-axis as shown in Figs. 1. The displacement of the rotor coordinate system with reference to the origin of the stator coordinate system is shown elsewhere, in Fig. 3.

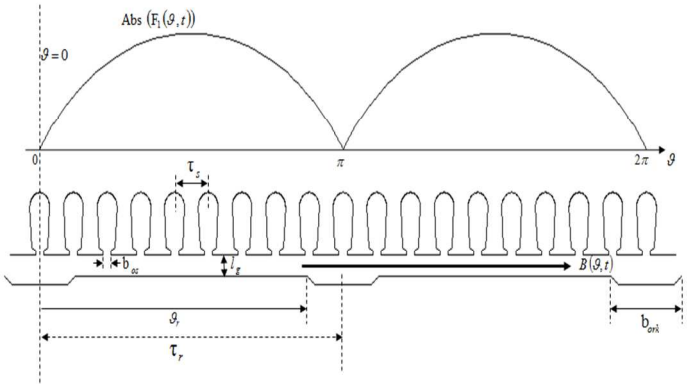

Fig. 3: Displacement of rotor coordinates system

The rotor is slotted (rotor cut-off opening) and the origin of rotor cut-off opening is displaced by the angle ϑ_r from the origin of stator slotting as shown in Fig. 3. Let $\Delta l_{g\,rk}(\vartheta-\vartheta_{rk})$ be the increase in airgap due to the rotor cut-off opening for any *k* stack rotor lamination, the effective airgap length for each of the stack rotor laminations at any given point can be expressed as

$$\begin{aligned} l_{gk_{eff}}(\vartheta)&=\Delta l_{g_s}(\vartheta)+\Delta l_{gkr}(\vartheta-\vartheta_{rk})+l_g \\ &=\frac{1}{\mathrm{f_s}(\vartheta)}+\frac{1}{\mathrm{f_{rk}}(\vartheta-\vartheta_{rk})}-l_g \end{aligned} \tag{17}$$

Taking into account the rotor cut-off opening effect by using the Carter's coefficient, the effective airgap length can be given as

$$l_{gk_{eff}}(\vartheta)=l_g\,\kappa_{cs}\,\kappa_{cr_k} \tag{18}$$

Here κ_{crk} is the Carter's coefficient that accounts for the rotor cut-off opening of any *k* rotor stack lamination having cut-off on the *q*-axis. The increase in airgap due to the rotor cut-off opening is given by

$$\Delta l_{g\,kr}(\vartheta-\vartheta_{rk})=l_g\,\kappa_{cs}(\kappa_{cr_k}-1) \tag{19}$$

The average airgap length and average airgap conductance for the Novel SynRM at any point ϑ, taking into account the slot opening on both stator and rotor sides of the airgap, are respectively obtained as

$$l_g(\vartheta,\vartheta_r)_{av}=\frac{1}{21}\left[l_g(\kappa_{cs}-1)+2\sum_{k=1}^{10}l_g(\kappa_{cs}-1)+l_g\kappa_{cs}(\kappa_{cr_k}-1)\right] \tag{20}$$

$$\sigma(\vartheta,\vartheta_r)_{av}=\frac{1}{\frac{1}{21}\left[l_g(\kappa_{cs}-1)+2\sum_{k=1}^{10}l_g(\kappa_{cs}-1)+l_g(\kappa_{cr_k}-1)\right]} \tag{21}$$

Let $\mathrm{f_s}(\vartheta)$ and $\mathrm{f_{rk}}(\vartheta-\vartheta_{rk})$ in (17) be periodic functions of which the periods are determined by the stator slot pitch and the rotor cut-off pitch respectively, they may be given in Fourier series as

$$\mathrm{f}_s(\vartheta)=a_o-\sum_{n=1}^{\infty}a_n\cos\,nQ_s\vartheta \tag{22}$$

$$\mathrm{f}_{rk}(\vartheta-\vartheta_{rk})=b_{ok}-\sum_{n=1}^{\infty}b_n\cos\,nN_r(\vartheta-\vartheta_{rk}) \tag{23}$$

Where a_o and b_{ok} are given in equations (24) and (25) respectively [25] and Q_s and N_r are the total number of stator slots and rotor cut-offs respectively.

$$a_o=\frac{1}{\kappa_{cs}\,l_g}=\frac{0.873}{l_g} \tag{24}$$

$$b_{ok}=\frac{1}{\kappa_{cr_k}\,l_g} \tag{25}$$

The Fourier series coefficients for the *n* harmonics are determined by using the conformal transformation of the

effect of stator slotting and rotor cut-off on the airgap flux density distribution [29]. One may obtain;

$$a_n, b_{nk} = \frac{\beta_{s,r}}{l_g} \mathrm{F}_n \left(\frac{\mathrm{b}_{os,rk}}{\tau_{s,r}} \right) \tag{26}$$

Here $\beta_{s,r}$ is a function of the ratio of stator slot opening (subscript "*s*") or rotor cut-off opening (subscript "*r*") to the airgap length and F_n is given as [29]

$$\mathrm{F}_n\left(\frac{\mathrm{b}_{os,rk}}{\tau_{s,r}}\right) = \frac{4}{n\pi}\left[0.5 + \frac{\left(\frac{n\,\mathrm{b}_{os,r}}{\tau_{s,r}}\right)^2}{0.78 - 2\left(\frac{n\,\mathrm{b}_{os,rk}}{\tau_{s,r}}\right)^2}\right] \sin\left(1.6\frac{\pi n\,\mathrm{b}_{os,rk}}{\tau_{s,r}}\right) \tag{27}$$

The ratios b_{os}/τ_s and b_{or}/τ_r are taken directly from the stator and rotor dimensions respectively. The Carter's coefficients, due to stator slot opening for the Novel SynRM, have been found to be 1.145.

Once the Fourier series coefficients a_n and b_n are found, the harmonic airgap conductance, which takes both sides of the stator slotting and rotor cut-off opening of the airgap into account, is obtained by using

$$\sigma(\vartheta,\vartheta_{rk}) = \frac{1}{l_g}\left\{\frac{1}{\kappa_{cs}\kappa_{crk}} - \sum_{n=1}^{\infty}\frac{a_n}{\kappa_{crk}}\cos n N_s\left(\frac{\vartheta}{P_1}\right) - \frac{b_n}{\kappa_{cs}}\cos n N_r\frac{(\vartheta-\vartheta_r)}{P_1} + a_n b_n\left[\cos n\left(\frac{(Q_s+N_r)}{P_1}\vartheta - \frac{N_r}{P_1}\vartheta_r\right) + \cos n\left(\frac{(Q_s-N_r)}{P_1}\vartheta + \frac{N_r}{P_1}\vartheta_r\right)\right]\right\} \tag{28}$$

It should be noted that (28) computes the harmonic airgap conductance related to the stator slot opening and rotor cut-off for a given *k* stack rotor lamination in the Novel SynRM. The proposed novel machine is composed of $2(k_1 + k_2 + \ldots + k_{10}) + k_v$) laminations. From (28), it is observed that the magnetic airgap conductance, which takes into account the slotting on both sides, as well as the stator slot opening and rotor cut-off for any *k* stack lamination, has harmonics related directly to the number of stator slots and rotor cut-offs and their geometry. The airgap conductance profiles for the Novel SynRM and the SynRM with cut-off on the rotor *q*-axis, obtained at rotor displacement angle of 45° elect, are shown in Fig. 4 (a).

Observing from Fig. 4 (a), it is noted that the stator slot openings and rotor cut-off opening are visible in both models. Fig. 4 (b) depicts the FFT results. The dominant airgap conductance harmonics are enlarged.

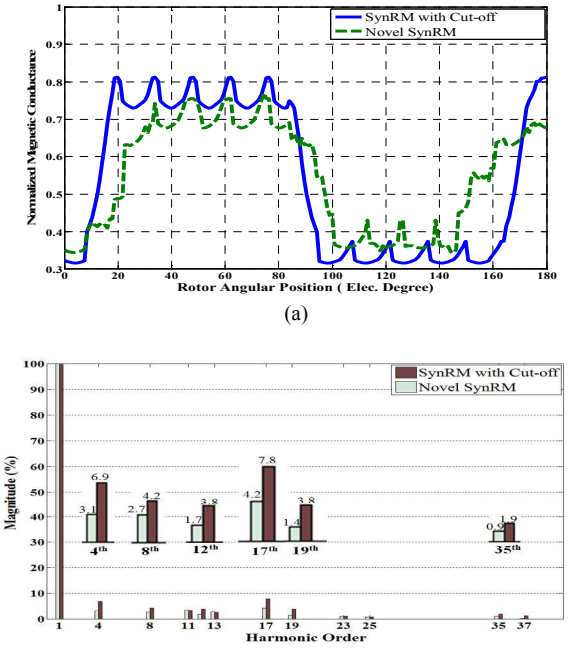

Fig. 4: Distribution of magnetic conductance, (a) magnetic conductance profiles, (b) FFT of the magnetic conductance profiles

IV. Finite Element Analysis Results

The comparison of torque behaviors for different loading current are shown in Figs. 5 (a) and (b).

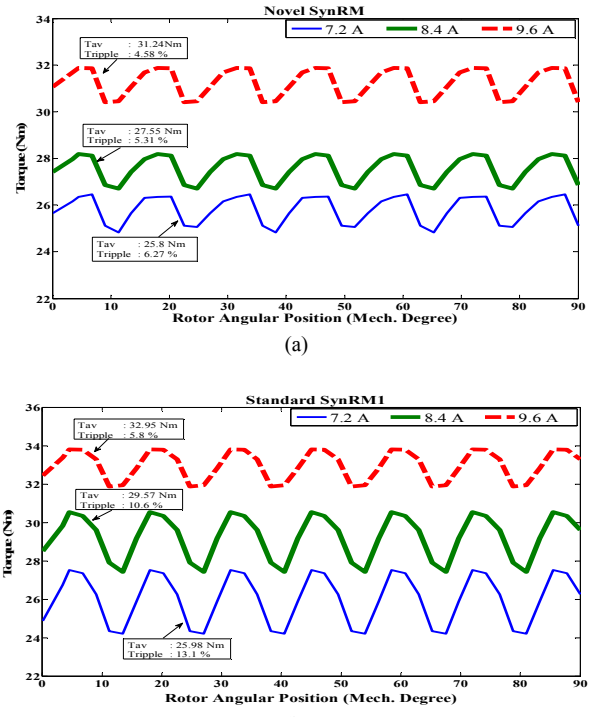

Fig. 5: Torque as function of rotor position, (a) Novel SynRM, (b) Standard SynRM1

The FEA were carried out at constant speed of 1500-rpm and constant frequency of 50-Hz. Both Standard SynRM1 and the Novel SynRM have three-phase double layer lap windings chorded by one slot. The windings are excited by 3-phase sinusoidal currents. The machines were run at the current space phasor angles of 55° *elec*. From Figs. 5 (a) and (b) , it is evident that the Novel SynRM has tremendously reduced the torque ripple from 13.1 %, 10.6 % and 5.8 % for the Standard SynRM1 down to 6.27 %, 5.31 % and 4.58 %, at the load current of 7.2 A, 8.4 A and 9.6 A respectively. The difference in torque average between the two SynRMs is insignificant.

V. Practical Validation

In this section, the experimental evaluation of the novel synchronous reluctance motor with sinusoidal anisotropic rotor is presented. The Novel SynRM is tested to validate the results obtained from FEA. The shaft torque as function of rotor position and its ripple content are obtained through the dynamic test.

A. Experimental Set-up

The experimental setting mainly comprises of the Novel three-phase SynRM coupled to a Wirbelstrombremse Siemens Eddy Current brake. The shaft torque, speed and mechanical power are measured by the rotary Magtrol's Model 3410 torque transducer with range from 0 to 50 Nm and a maximum speed of 4000 r/min. The torque transducer powers the torque meter and utilizes high speed Digital Signal Processing (DSP) to display torque, speed and mechanical power. The Dranetz PowerVisa 4400 three-phase power analyzer, equipped with eight independent channels, is utilized for advanced power monitoring and storage. The Tektronix TPS 2024 four channels digital oscilloscope is used to analyse both electrical and mechanical parameters of interest. The SynRM is started by means of an industrial drive of ACS880 type. Fig. 6 shows the experimental setup rig photo.

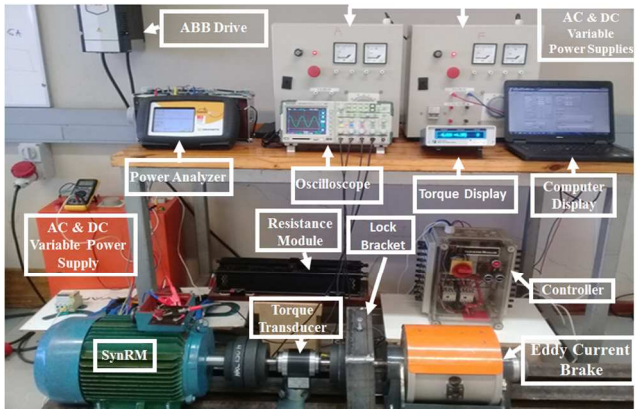

Fig. 6: Experimental setup rig photo

B. Analysis of results

The torque profiles as function of rotor position for the Novel SynRM and Standard SynRM1 are shown in Figs.7 (a) and (b) respectively. Both Synchronous reluctance motors were run at constant speed of 1500-rpm and were subjected to three different loading conditions. The Wirbelstrombremse Siemens Eddy current brake shown in Fig. 12 was only able to provide a maximum load torque of 32 Nm. Due to this limitation, the SynRMs were loaded only up to 80% of their rated power.

The SynRMs have three-phase double layer lap windings which were fed by an industrial drive that provided the most needed starting and accelerating torques. The setting of the drive abled the SynRMs to run at the current space phasor angle of 55° *elec* during the different loading conditions.

Observing the practical results illustrated from Figs. 7 (a) and (b), it is evident that the Novel SynRM has tremendously reduced the torque ripple from 12.48 %, 9.26 % and 4.78 % for the Standard SynRM1 down to 5.4 %, 4.3 % and 3.2 %, with the loading capacity of 60 %, 70 % and 80 % respectively. These results are close to the results obtained from the FEA, and the comparison between practical and simulation results are depicted in table 2.

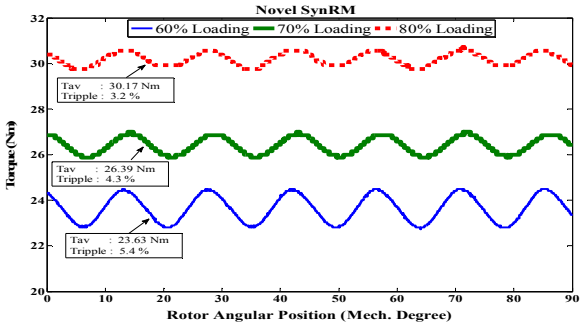

(a)

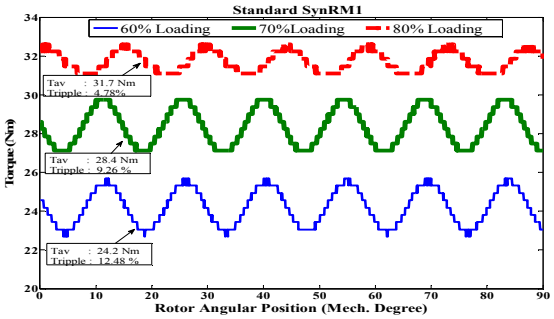

(b)

Fig. 7: Shaft torque profiles, (a) Novel SynRM, (b) Standard SynRM

TABLE II
COMPARISON TORQUE AND TORQUE RIPPLE

	Novel SynRM				Standard SynRM1			
	FEA		Measured		FEA		Measured	
Load (A)	T_{av} (Nm)	T_{ripple} (%)	T_{av} (Nm)	T_{ripple} (%)	T_{av} (Nm)	T_{ripple} (%)	T_{av} (Nm)	T_{ripple} (%)
7.2	25.8	6.3	23.6	3.2	25.9	13.1	24.2	12.5
8.4	27.5	5.3	26.4	4.3	29.5	10.6	28.4	9.2
9.6	31.2	4.6	30.2	5.4	32.9	5.8	31.7	4.8

The FFT was performed on torque profiles in Figs 5 and 6, and the results are depicted from table 3 to table 5. The FFT results
evidenced that the torque harmonics that are due to stator and rotor anisotropy are visibly.

TABLE III
COMPARISON OF TORQUE HARMONICS AT 7.2 A

	Novel SynRM		Standard SynRM1	
Harmonic Order	FEA	Measured	FEA	Measured
6th	2.5 %	2.5 %	2.3 %	2.4 %
12th	3.5 %	4.2 %	6.3 %	8.2 %
18th	5.0 %	6.1 %	9.8 %	12.8 %
24th	2.8 %	2.7 %	2.4 %	2.5 %
30th	1.7 %	1.8 %	1.4 %	1.5 %
36th	3.5 %	4.2 %	5.6 %	7.2 %
48th	1.2 %	1.5 %	1.2 %	1.5 %

TABLE IV
COMPARISON OF TORQUE HARMONICS AT 8.4 A

	Novel SynRM		Standard SynRM1	
Harmonic Order	FEA	Measured	FEA	Measured
6th	2.6 %	2.8 %	2.5 %	2.6 %
12th	2.5 %	3.1 %	5.6 %	6.7 %
18th	4.2 %	5.4 %	10.2 %	12.2 %
24th	1.4 %	1.7 %	1.5 %	1.7 %
30th	1.4 %	1.7 %	1.2 %	1.4 %
36th	2.1 %	2.7 %	4.4 %	5.2 %
48th	1.2 %	1.3 %	1.2 %	1.3 %

TABLE V
COMPARISON TORQUE HARMONICS AT 9.6 A

	Novel SynRM		Standard SynRM1	
Harmonic Order	FEA	Measured	FEA	Measured
6th	2.4 %	2.8 %	2.7 %	2.6 %
12th	1.3 %	1.9 %	6.7 %	6.2 %
18th	2.4 %	3.6 %	12.9 %	11.9 %
24th	2.1 %	2.6 %	2.5 %	2.4 %
30th	1.1 %	2.2 %	2.2 %	2.3 %
36th	0.8 %	1.1 %	3.3 %	3.0 %
48th	0.9 %	1.2 %	1.1%	1.2 %

The 12th harmonics are caused by the rotor slotting, while the 18th, 36th and 54th are due to the stator slotting. Observing the measured results in the above tables, it is noted that the Novel SynRM has significantly dropped the 12th torque harmonic from 8.2 %, 6.7 % and 6.2 % for the Standard SynRM1, down to 4.2 %, 3.1 % and 1.9 %, at loading condition of 60 % (7.2 A) , 70 % (8.4 A) and 80 % (9.6 A) respectively. For the same loading pattern, the Novel SynRM has tremendously dropped the 18th torque harmonic from 12.8 %, 12.2 % and 11.9 % for the Standard SynRM1, down to 6.1 %, 5.4 % and 3.6 %. The torque harmonic due to magnetic saturation of the rotor tangential and radial bridges are well visible in the FFT results, as it was in the case of FEA results presented in the previous section. There is an agreement between the FEA and measured results.

VI. CONCLUSION

Design aspects and considerations of the Novel SynRM with sinusoidal rotor lamination shape in the axial direction have been presented in this paper. This paper has also presented the analytical expression that should be used to compute the harmonic airgap conductance related to the stator slot opening and rotor cut-off for a given *k* stack rotor lamination in the novel SynRM. The validation of theoretical analysis and simulation results has been carried out through practical measurements. Both FEA and measured results showed that the torque produced by the Novel SynRM has less ripple contents than the Standard SynRM1, while still maintaining the average torque. The significant reduction of torque ripple content in the Novel SynRM was justified by the mitigation of some torque harmonics caused by stator slotting and rotor anisotropy.

REFERENCES

[1] A. Fratta, and A. Vagati, "A reluctance motor drive for high dynamic performance applications. *IEEE-IAS annual meeting*, 1987, Atlanta, USA

[2] A. Fratta, G. P Troglia, A. Vagati, and F. Villata, "Evaluation of torque ripple in high performance synchronous reluctance motors". *Record of IEEE Industry Application Society Annual Meeting*, I: 163-170, October, Toronto, Canada, 1993

[3] D. A Staton, T. J. E. Miller, and S. E. Wood, "Maximizing the saliency ratio of the synchronous reluctance motor", *IEE Proc- Electric Po. Appl,* Vol. 140. no 4, pp. 249-259, July. 1993

[4] N. Bianchi and S. Bolognani, "Reducing Torque Ripple in PM Synchronous Motors by Pole Shifting". *Proceeding of International Conference on Electrical Machines, ICEM.* Aug. Helsinki, 2000.

[5] A Fratta, A. Vagati, F. Villata, G. Franceschini and C. Petrache, " Design comparison between induction and synchronous reluctance motors", *Proceeding of International Conference on Electrical Machines, ICEM.* Sept. 1994, Vol. 3, pp. 329-334.

[6] M. J Kamper, F. S. Van der Merwe and S. Williamson, "Direct finite element design optimization of the cage-less reluctance synchronous machine", *IEEE Trans. on Energy Con.*, Vol. 11, IS, 3, Sept. 1996, pp: 547-555.

[7] E.C Lovelace, "Optimization of a magnetically saturable IPM Sync. Mac. Drive", *PhD, Dept. of Elec. Eng. & Comp. Sci., MIT*, 2000.

[8] A. Vagati, G. Franceschini, I Morongiu and G.P. Troglia, "Design criteria of high performance synchronous reluctance motors*". Ind. Appl., Annual Meet*. 4-9 Oct., 1992, Vol.1, pp: 66-73.

[9] J. K. Kostko, "Poly-phase Reaction Synchronous Motor" *Journal of A.I.E.E.*, Vol. 42, 1923, pp. 1162-1168.

[10] T.A. Lipo, T. J.E Miller, A. Vagati, I. Boldea, L. Malesani and T. Fukao, "Synchronous Reluctance Drives*", Tutorial IEEE-IAS Annual Meeting*, Denver, CO, Oct. 1994

[11] I. Boldea, "Reluctance synchronous machines and drives", Oxford, UK: Clarendon Press, 1996.

[12] A. Vagati, "The Synchronous Reluctance Solution: A New Alternative in a.c. Drives", *20th Conference on Industrial Electronics, Control and Instrumentation (IECON 1994),* Bologna, Italy, 1994.

[13] T. A. Lipo, "Synchronous reluctance machines- a viable alternative for AC drives? *", Electric Machines and Power Systems*, Vol. 19, no. 6, pp. 659-671. 1991

[14] N. Bianchi, S. Bolognani, D. Bond and M. D. Pre', Rotor Flux-barrier Design for Torque Ripple Reduction in Synchronous Reluctance Motors. *Proc. 41th IEEE Conf. On Industry Applications*, 2006, 1193-1200.

[15] S. Talebi, P. Niazi and H. A Toliyat, "Design of Permanent Magnet-assisted Synchronous Reluctance Motors Made Easy", *Ind. Appl. Conf., 2007, 42nd IAS An. Meet*, 23-27 Sept. 2007, pp. 2242-2248.

[16] H. A. Toliyat, S.P Waikar, and T. A. Lipo, " Analysis and Simulation of Five Phase Synchronous Reluctance Machines Including Third Harmonic Airgap MMF, " *IEEE Transaction on Industry Applications*, vol. 34, pp, 332-339, 1998.

[17] N. Bianchi, S. Bolognani, D. Bon, and M. D. Pre', Rotor Flux-barrier Design for Torque Ripple Reduction in Synchronous Reluctance and

PM-Assisted Synchronous Reluctance Motors. *IEEE Trans. on Ind. Appl.*, vol. 45, Issue 3, May-June 2009, pp. 921-928.
[18] X. L. Bomela and J. Kamper, Effect of Stator Chording and Rotor Skewing on Performance of Reluctance Synchronous Machines. *IEEE Transaction on Industry Application,* Vol. 38. no. 1. January/February 2002.
[19] A. Vagati, M. Pastorelli, G. Franceschini and C. Petrache, Design of low-torque-ripple Synchronous Reluctance Motors. *Annual Meeting, Proc. IEEE Conf Industry Applications*, *LA,* 1997, 287-293.
[20] E. Chiricozzi, G. Conti, F. Parasiliti, and M. Villani," Design solutions to optimize torque ripple in synchronous reluctance motors", *Proceedings in International Electrical Machines,* 1996, Vigo, Spain.
[21] M. Sanada, K. Hiramato, S. Morinoto, and Y. Takeda. "Torque Ripple Improvement for Synchronous Reluctance Motor Using Asymmetric Flux Barrier Arrangement". *Proc. IEEE Ind. App. Soc. Annual Meeting*, 12-16 Oct. 2003.
[22] T. Lange, B. Kerdsup, C. Weiss, and R. W. De Doncker, "Torque ripple reduction in reluctance synchronous machines using an asymmetric rotor structure. *7th IET International Conference on Power Electronics, Machines and Drives (PEMD),* 2014, Manchester, UK
[23] W. Zhao, T. A. Lipo, and B. Kwon, "\Material-efficient permanent-magnet shape for torque pulsation minimization in SPM motors for automotive applications. *IEEE Trans. On Industrial Applications*. Vol. 69, pp. 5779-5787, Jan, 2014.
[24] M. Muteba, B. Twala, D. V. Nicolae, " Torque ripple minimization in synchronous reluctance motor using a sinusoidal rotor shape", *22nd IEEE International Conference on Electrical Machines*, Lausanne, Switzerland, 2016, pp. 606-611
[25] H, Grop, "Investigation of AC electrical machines stators with fractional conductor windings, Stockholm: *KTH Royal Institute of Technology*, 2010.
[26] B. Xiaohua, L. Na, F. Yong, and L. Fuying, "Novel method of evaluation of Carter factor for closed slot submersible motor including fringing effect and magnetic saturation". *Transaction on China Electrotechnical Society,* 30(12), pp. 220-227, 2015
[27] H. Vu Xuan, D. Lahaye, H. Polinder, and J. A. Ferreira,." Influence of stator slotting on the performance of permanent-magnet machnines with concentrated windings", Dlft: *Report of the Department of Applied Mathematics Analysis*, Delft University of Technology, 2012.
[28] F. W. Carter, "The magnetic field of the dynamo-electric machine", *Journal of the Institution of Electric Engineeris,* 64(359), pp. 1115-1138, 1926
[29] B. Heller, and V. Hamata, "Harmonic field effects in induction machines" *New York, USA*: Elsevier Scientific Publishing Company, 1977.

Mbika Muteba received the Associate Degree of applied science and technology in electrical engineering from higher institute of technology, Katanga, DRC, in 1996. After ten years of industrial experience in electrical machines, machines drives, primary and secondary power distribution networks both in DRC and South Africa, he joined the Tshwane University of Technology, South Africa, in 2006. He received the Bachelor's and Master's degrees of Technology in Electrical Engineering in 2008 and 2013, respectively. He is has his final phase of completing his PhD in Electrical and Electronic Engineering at the University of Johannesburg. Muteba is employed on permanent basis as a lecturer in the Department of Electrical and Electronic Engineering Technology at the University of Johannesburg. His research interests are design and control of electrical machines for future Electric and Hybrid Electric Vehicles.

Bhekisipho Twala is a Professor in Artificial Intelligence and Statistical Science and the Director of the newly established Institute for Intelligent Systems at the University of Johannesburg (UJ) in South Africa. Before then, he was Head of the Electrical and Electronic Engineering Science Department at UJ and Principal Research Scientist at the Council of Science and Industrial Research (CSIR) within the Modelling and Digital Science Unit.
His research work involved an expanded swath of data, analytics, and optimization approaches that brings a more complete understanding of digital customer experiences.
Prof Twala's current work involves promoting and conducting research in artificial intelligence within the electrical and electronic engineering science fields and developing novel and innovative solutions to key research problems in these areas. He earned his Bachelor's degree in Economics and Statistics from the University of Swaziland in 1993; followed by an MSc in Computational Statistics from Southampton University (UK) in 1995; and then a PhD in Machine Learning and Statistical Science from the Open University (UK) in 2005.
Prof. Twala was a post-doctoral researcher at Brunel University in the UK, mainly focusing on empirical software engineering research and looking at data quality issues in software engineering. His broad research interests include multivariate statistics, classification methods, knowledge discovery and reasoning with uncertainty, sensor data fusion and inference, and the interface between statistics and computing. He has particular interests in applications in finance, medicine, psychology, software engineering and most recently in robotics and has published over 70 scientific papers. Prof. Twala has a wide ranging work experience to organizations ranging from banks, through universities, to governments. He is currently an associate editor of the Intelligent Data Analysis Journal, Journal of Computers, International Journal of Advanced Information Science and Technology, International Journal of Big Data Intelligence, Journal of Image and Data Fusion, Journal of Information Processing Systems, and a fellow of the Royal Statistical Society.
Other professional memberships include the Association of Computing Machinery (ACM); the Chartered Institute of Logistics and Transport (CIT), South Africa and a senior member of the Institute of Electrical and Electronics Engineers (IEEE).

Dan Valentin Nicolae, born in Romania 18/09/1948, has got his first degree Master in (Applied) Electronic Engineering in 1971 from University Polytechnic of Bucharest, Romania. Between 1971 and 1975 he was with Institute for Nuclear Technologies as design engineer, than in 1975 he joined National Institute for Scientific and Technical Creativity – Avionics Branch in Bucharest Romania as principal researcher. In 1998, D. V. Nicolae joined Tshwane University of Technology as lecturer for heavy current subjects. In 2000 he started his research activity in TUT with a stage in France; with this opportunity he started his PhD which has been finalized in 2004. In 2015 he joined University of Johannesburg. Presently, Prof. DV Nicolae is involved in research in power converters for power systems, electric machines, power systems and renewable energy.